Materials Research Letters

ISSN: 2166-3831 (Online) Journal homepage: www.tandfonline.com/journals/tmrl20

Probing the effect of intragranular premature κ-carbide on incipient plasticity behavior in austenite-based Fe-Mn-Al-(Cr)-C steels

Jianlei Zhang, Yuxiang Liu, Conghui Hu, Ahmed Addad, Alex Montagne, Gang Ji, Changjiang Song & Qijie Zhai

To cite this article: Jianlei Zhang, Yuxiang Liu, Conghui Hu, Ahmed Addad, Alex Montagne, Gang Ji, Changjiang Song & Qijie Zhai (2022) Probing the effect of intragranular premature κ-carbide on incipient plasticity behavior in austenite-based Fe-Mn-Al-(Cr)-C steels, Materials Research Letters, 10:3, 141-148, DOI: 10.1080/21663831.2022.2027034

To link to this article: https://doi.org/10.1080/21663831.2022.2027034

© 2022 The Author(s). Published by Informa UK Limited, trading as Taylor & Francis Group.

View supplementary material

Published online: 31 Jan 2022.

Submit your article to this journal

Article views: 1525

View related articles

View Crossmark data

Citing articles: 5 View citing articles

Full Terms & Conditions of access and use can be found at
https://www.tandfonline.com/action/journalInformation?journalCode=tmrl20

MATER. RES. LETT.
2022, VOL. 10, NO. 3, 141–148
https://doi.org/10.1080/21663831.2022.2027034

ORIGINAL REPORTS

OPEN ACCESS

Probing the effect of intragranular premature κ-carbide on incipient plasticity behavior in austenite-based Fe-Mn-Al-(Cr)-C steels

Jianlei Zhang[a,b,c], Yuxiang Liu[a,b], Conghui Hu[a,b], Ahmed Addad[c], Alex Montagne[d], Gang Ji[c], Changjiang Song[a,b] and Qijie Zhai[a]

[a]Center for Advanced Solidification Technology (CAST), School of Materials Science and Engineering, Shanghai University, Shanghai, People's Republic of China; [b]State Key Laboratory of Advanced Special Steel, School of Materials Science and Engineering, Shanghai University, Shanghai, People's Republic of China; [c]Univ. Lille, CNRS, INRAE, Centrale Lille, UMR 8207 - UMET - Unité Matériaux et Transformations, Lille, France; [d]Arts et Metiers Institute of Technology, MSMP, HESAM Université, Lille, France

ABSTRACT

The effect of nanoscale intragranular premature κ-carbide precipitates, having an ordered structure but without chemical partitioning, on the incipient plasticity behavior of austenite in Fe-Mn-Al-(Cr)-C low-density steels was investigated by nanoindentation. We found that the incipient plasticity was dominated by a heterogeneous dislocation nucleation mechanism via atom-vacancy exchange. Although the content of κ-carbide decreased with Cr addition, its negligible effect on incipient plasticity strength was witnessed by the slightly increased shear stress for dislocation nucleation. Comparatively, the increased interstitial C atoms with Cr content in austenite enhanced lattice cohesions which impeded the nucleation events by increasing the requisite shear stress.

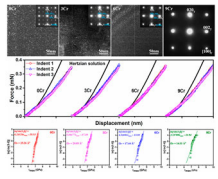

ARTICLE HISTORY
Received 16 November 2021

KEYWORDS
Fe-Mn-Al-C low-density steel; premature κ-carbide; dislocation nucleation; nanoindentation; charge transfer

IMPACT STATEMENT

Despite being one of the most important strengthening phases, nanoscale premature κ-carbide precipitates surprisingly have a negligible effect on incipient plasticity of austenite in Fe-Mn-Al-(Cr)-C low-density steels.

1. Introduction

Nanoscale κ-carbide is considered to be one of the most important strengthening phases in Fe-Mn-Al-C low-density steels [1–3]. For example, it has been shown to enhance yield strength in austenite-based steels by 340–480 MPa [2,3]. This enhancement was attributed to an ordering induced strengthening [3] whereby matrix dislocation sheared an ordered κ-carbide precipitate to create an antiphase boundary on the slip plane of the precipitate [4]. κ-carbide precipitation was also considered critical for planar dislocation glide during plastic deformation in austenite [2,5]. Indeed, incipient plastic deformation, i.e. the onset of permanent deformation, can be induced by the dislocation nucleation during elastic-plastic transformation [6–11]. It was suggested that the transition from atomistic deformation to continuum-level plasticity may be closely associated with dislocation nucleation [6]. However, no reports on incipient plasticity behavior were available till now, limiting one's understanding on the role of κ-carbide on plasticity.

Instrumented nanoindentation has been found to be a powerful tool to assess incipient plasticity associated with different dislocation nucleation mechanisms in metallic materials [9–14]. The first pop-in event or split-off point

CONTACT Gang Ji gang.ji@univ-lille.fr Univ. Lille, CNRS, INRAE, Centrale Lille, UMR 8207 - UMET - Unité Matériaux et Transformations, F-59000 Lille, France; Changjiang Song riversong@shu.edu.cn Center for Advanced Solidification Technology (CAST), School of Materials Science and Engineering, Shanghai University, Shanghai 200444, People's Republic of China; State Key Laboratory of Advanced Special Steel, School of Materials Science and Engineering, Shanghai University, Shanghai 200444, People's Republic of China

Supplemental data for this article can be accessed here. https://doi.org/10.1080/21663831.2022.2027034

© 2022 The Author(s). Published by Informa UK Limited, trading as Taylor & Francis Group.
This is an Open Access article distributed under the terms of the Creative Commons Attribution License (http://creativecommons.org/licenses/by/4.0/), which permits unrestricted use, distribution, and reproduction in any medium, provided the original work is properly cited.

deviated from theoretical elastic deformation in a load-displacement (*P-h*) curve during indentation loading, are generally considered to be the response to dislocation nucleation at the incipient plasticity stage [8,10,14]. It was found in a dual-phase Fe-Mn-C-Si steel that dislocations nucleating earlier in large ferrite grains than in small ferrite and austenite grains, were responsible for incipient plasticity [14]. Nanoindentation tests also indicated a homogeneous dislocation nucleation mechanism in austenite grains of Fe-21Mn-11Al-1.5C-2Si (wt. %) steel spanning a range of processing conditions from solution, aging to thermo-mechanical treatments [12].

Our recent work [15] has highlighted a new intragranular premature κ-carbide (2–3 nm in particle size) in Fe-20Mn-9Al-3Cr-1.2C (wt. %) low-density steel. As compared with the well-known coarsened κ-carbide [3,16], it has an ordered $L'1_2$ structure but without detectable chemical partitioning with austenite at near-atomic scale. This means that the ordered $L'1_2$ structure of the intragranular κ-carbide could be approximated as an FCC structure with an interstitial C atom occupying the body-centered octahedral position. Regarding the effect of interstitial atoms on incipient plasticity, it was suggested that dissolving 0.5 at. % C and 1.0 at. % N into a FeMnCoCr high entropy alloy (HEA) increased the activation volume and maximum shear stress necessary for the homogeneous dislocation nucleation to be triggered by a thermally activated displacement of a single principal atom [10]. However, Y.X. Ye et al. [9] proposed a heterogeneous dislocation nucleation mechanism via cooperative migration of multiple atoms in a NbTiZrHf HEA, where the interstitial O and N atoms induced an increase of critical shear stress but with no significant effect on activation process. Thus, in this work, we aimed to probe the effect of such an intragranular premature κ-carbide on incipient plasticity in austenite-based Fe-Mn-Al-(Cr)-C steels using nanoindentation. Because of the suppression effect of the Cr alloying element on precipitation of κ-carbide [17–19], it was intentionally added in order to have representative sample states with and without κ-carbide.

2. Materials and methods

Four Fe-20Mn-9Al-(0, 3, 6 and 9) Cr-1.2C (wt. %) low-density steel samples, hereafter referred to as 0Cr, 3Cr, 6Cr and 9Cr, were studied. As detailed in our previous works [20,21], they were prepared by induction melting and centrifugal casting in an argon atmosphere with cooling rates in excess of 10^3 K/s (namely near-rapid solidification). Scanning electron microscopy (SEM) characterization was carried out using a JEOL JSM-7800F microscope equipped with an electron backscatter diffraction (EBSD) detector and dedicated Channel 5 software was used for post- data treatment. Transmission electron microscopy (TEM) characterization was done using a FEI Tecnai G2-20 twin microscope, operated at 200 kV and a Thermofisher Titan Themis 60-300 microscope, operated at 300 kV. The latter was equipped with a probe aberration corrector for acquiring (high-resolution) scanning TEM ((HR)STEM) high-angle annular dark-field (HAADF) images. TEM specimens were prepared by twin-jet electrolytic polishing. Atomic probe tomography (APT) was performed using a local electrode atom probe instrument (CAMECA LEAP 4000 XHR), in laser-pulsed mode with a repetition rate of 200 kHz, a pulse fraction of 15%, and a specimen temperature of 50 K. APT specimen was prepared by standard two-step electro-polishing. A peak decomposition algorithm in IVAS 3.6.8 software was used to resolve peak overlapping among Fe, Al and Cr at 27 Da in mass spectrum for improving counting statistics [22]. Quantitative chemical composition was also examined by an electron probe micro-analysis (EPMA)-8050G instrument, operated at 15 kV.

Mechanical properties of austenite were measured by an MTS XP nanoindenter, equipped with a Berkovich tip with a constant loading rate of 0.05 s^{-1}. One hundred indentations separated by 10 μm were tested, addressing thus the influence of different austenite grain orientations. The data of indentation completely realized within austenite matrix was used for further analysis. Bader charge transfer was calculated using density functional theory (DFT) implemented in a Vienna ab initio simulation package (VASP). More description of the nanoindentation experiments and calculation can be found in the Supplementary Information.

3. Results and discussion

As shown in Figure 1(a-d), the volume fractions of the island-like ferrite phase in the 0Cr, 3Cr, 6Cr and 9Cr samples were respectively, 3%, 8%, 17% and 27%. Figure 1(e-g) indicate that the nanoscale intragranular κ-carbides are present in the austenite matrix of all the 0Cr, 3Cr and 6Cr samples and their average sizes were estimated as $\sim$5 nm, $\sim$3 nm and $\sim$1 nm, respectively. The classical cube-on-cube orientation relationship between κ-carbides and γ-austenite of $[100]_\kappa$ // $[100]_\gamma$ and $(001)_\kappa$ // $(001)_\gamma$ [1] is confirmed by selected-area electron diffraction (SAED) patterns (insets in Figure 1(e-g)). No superlattice reflection indicates that the existence of intragranular κ-carbides is invisible in the 9Cr sample (Figure 1(h)). Thus, the increase of Cr content leads to an increase in the ferrite content and a suppression of intragranular κ-carbide precipitation in austenite.

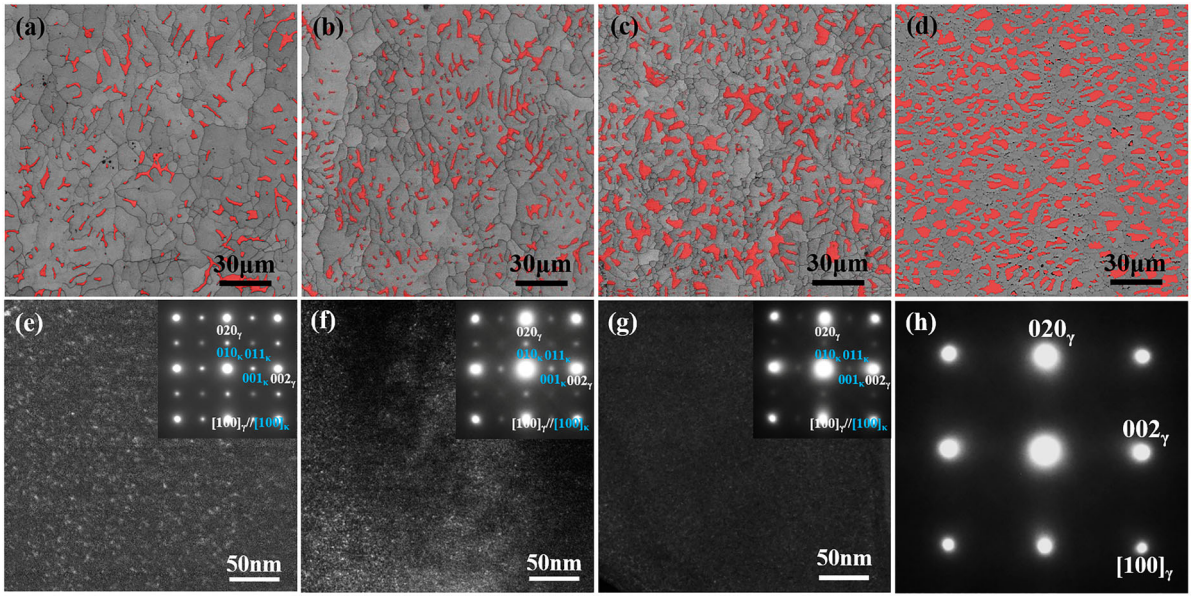

Figure 1. SEM/EBSD phase maps of the 0Cr (a), 3Cr (b), 6Cr (c) and 9Cr (d) samples, red and gray contrasts represent ferrite and austenite phases, respectively; TEM dark-field images of intragranular κ-carbide precipitates using $(001)_\kappa$ reflection in austenite of the 0Cr (e), 3Cr (f) and 6Cr (g) samples, respectively; (h) is $[100]_\gamma$ SAED pattern of austenite in the 9Cr sample. Insets in (e-g) are corresponding $[100]_\gamma$ SAED patterns.

Consistent with our results from the 3Cr sample [15], the structure and chemistry of nanoscale intragranular κ-carbide are better revealed by HRSTEM-HAADF and APT, respectively. For example, the ordered κ-carbide domains in the austenite matrix of the 0Cr sample, marked by red circles in Figure 2 (a), are clearly identified using FFT patterns. According to the simulated STEM-HAADF images in Figure 2(b), these κ-carbides have an ordered $L'1_2$ structure, assuming the non-stoichiometric C atom is located at the body-center octahedral site of the FCC structure. The APT result in Figure 2(c) shows the uniform distributions of all the Fe, Mn, Al and C constituent elements. The corresponding μ values (Figure 2(d)) of all the elements are close to 0, further indicating that they are randomly distributed on a near-atomic scale in the austenite [23,24]. It is confirmed here that the near-rapid solidification process resulted in the formation of intragranular premature κ-carbides in all the 0Cr, 3Cr [15] and 6Cr (result not given) samples.

Figure 3 shows that no significant pop-in events are observed in any of the samples tested by nanoindentation (the partial enlarged figures are shown in Figure S2 of Supplementary Imformation), suggesting a smooth and continuous deformation behavior. This could be caused by the high solid solution C content, which reduces the mean free path of mobile Shockley partial dislocations hence limiting plastic flow during deformation [10]. Providing that initial elastic deformation of the indented material follows the relation obtained by the Hertzian contact mechanics model [25], the deviation of the measured *P-h* curve from the Hertzian curve can be defined as the onset of plasticity [10,14,26,27]. Based on this model, the elastic response from a specimen surface layer is expressed by:

$$P = \frac{4}{3} E_r R_i^{\frac{1}{2}} h^{\frac{3}{2}} \tag{1}$$

where P is the applied load, R_i is the tip radius of the indenter ($\sim$200 nm, identified by fitting the initial elastic portion of the *P-h* curves with the Hertzian contact law [28]), h is the displacement of indent and E_r is the reduced modulus given by:

$$\frac{1}{E_r} = \frac{1 - v_i^2}{E_i} + \frac{1 - v_s^2}{E_s} \tag{2}$$

where E and v are the Young's modulus and Poisson's ratio, respectively. The subscripts i and s represent the indenter and sample, respectively. In this work, E_i, v_i and v_s are 1141 GPa [27], 0.07 [27] and 0.33 [29], respectively, and the E_s of different samples are shown in Table 1.

Table 1. The measured Young's modulus E, reduced modulus E_r, range of τ_{max} and average $\bar{\tau}_{max}$ of the studied samples.

Samples	E (GPa)	E_r (GPa)	Range of τ_{max} (GPa)	$\bar{\tau}_{max}$ (GPa)
0Cr	191.94 ± 2.33	181.33 ± 1.85	6.67–7.36	7.06 ± 0.20
3Cr	188.55 ± 2.80	178.62 ± 2.24	6.71–7.50	7.09 ± 0.25
6Cr	194.47 ± 2.72	183.34 ± 2.15	6.81–7.54	7.18 ± 0.22
9Cr	192.29 ± 2.55	181.61 ± 2.02	6.86–7.80	7.18 ± 0.26

To quantitatively analyze the elastic-plastic deformation of austenite with and without κ-carbide, the maximum shear stress (τ_{max}) beneath the indenter required

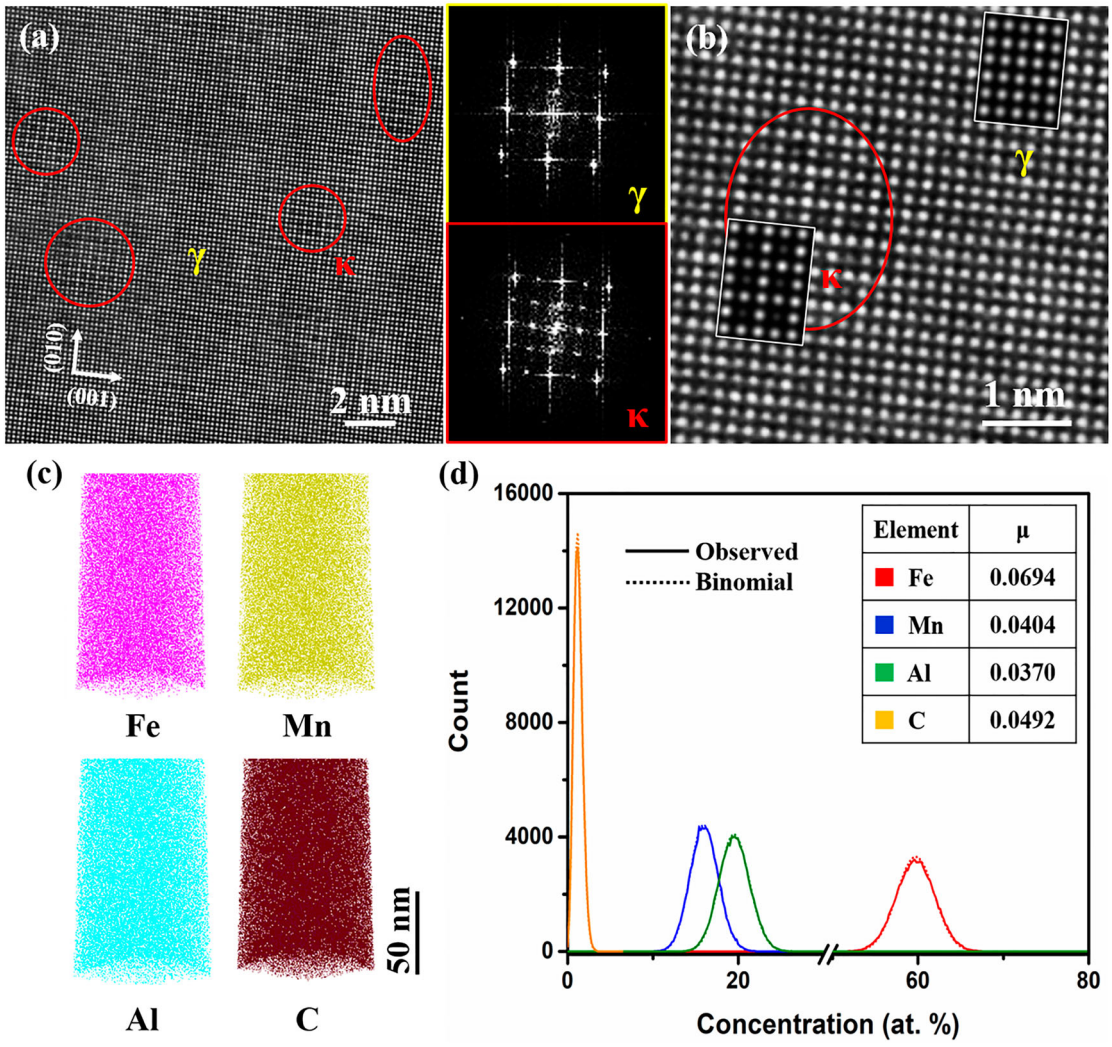

Figure 2. (a) HRSTEM-HAADF images of austenite in the 0Cr sample along the $[100]_\gamma$ orientation, insets are corresponding FFT patterns of austenite and κ-carbide, some regions containing κ-carbide are marked by red circles; (b) zoom-in image from (a), overlapped are simulated HRSTEM-HAADF images using κ-carbide ($E2_1$ Fe_3AlC) and austenite (FCC Fe) structural models; (c) Fe, Mn, Al and C elemental maps by APT characterization; (d) corresponding frequency distributions of the observed experimental data (solid line) fitted by the binomial simulation (dotted line), and the values of the normalized homogenization parameter μ are in inserted table in (d).

to trigger incipient plasticity can be calculated from [25]:

$$\tau_{max} = \frac{0.31}{\pi}\left(\frac{6PE_r^2}{R_i^2}\right)^{\frac{1}{3}} \tag{3}$$

where P is the load at which incipient plasticity occurs. The τ_{max} values (Table 1), can be determined from the P-h curves of each sample. It is clear that τ_{max}slightly increases with Cr content (the range of calculated τ_{max} values is shown in Figure S3 of Supplementary Information). Since the nanoscale intragranular κ-carbides are uniformly distributed in austenite (see Figures 1 and 2) and the radius of the indenter tip is much larger than the distance between κ-carbides, the incipient plasticity strength is thus the reliable response to the overall mechanical properties of austenite. The fact that the volume fraction of intragranular premature κ-carbide decreases with increasing Cr content (Figure 1) indicates that other factor than the presence of intragranular premature κ-carbides is dominating the τ_{max}, as will be discussed below.

In addition, cumulative probability f correlated with τ_{max} on the onset of incipient plasticity, is used to investigate the activation volume (Ω_v) for dislocation nucleation by Schuh's model [6,28]:

$$\ln[-\ln(1-f)] = \frac{\Omega_v}{kT}\tau + \beta \tag{4}$$

where k is the Boltzmann constant, T is the temperature and β is a weak function of shear stress. According to Equation (4), the slope $\frac{\Omega_v}{kT}$ can be determined by plotting and fitting ln[-ln(1-f)] vs. τ. Accordingly, the Ω_v of each sample can be deduced, as shown in Figure 3(b).

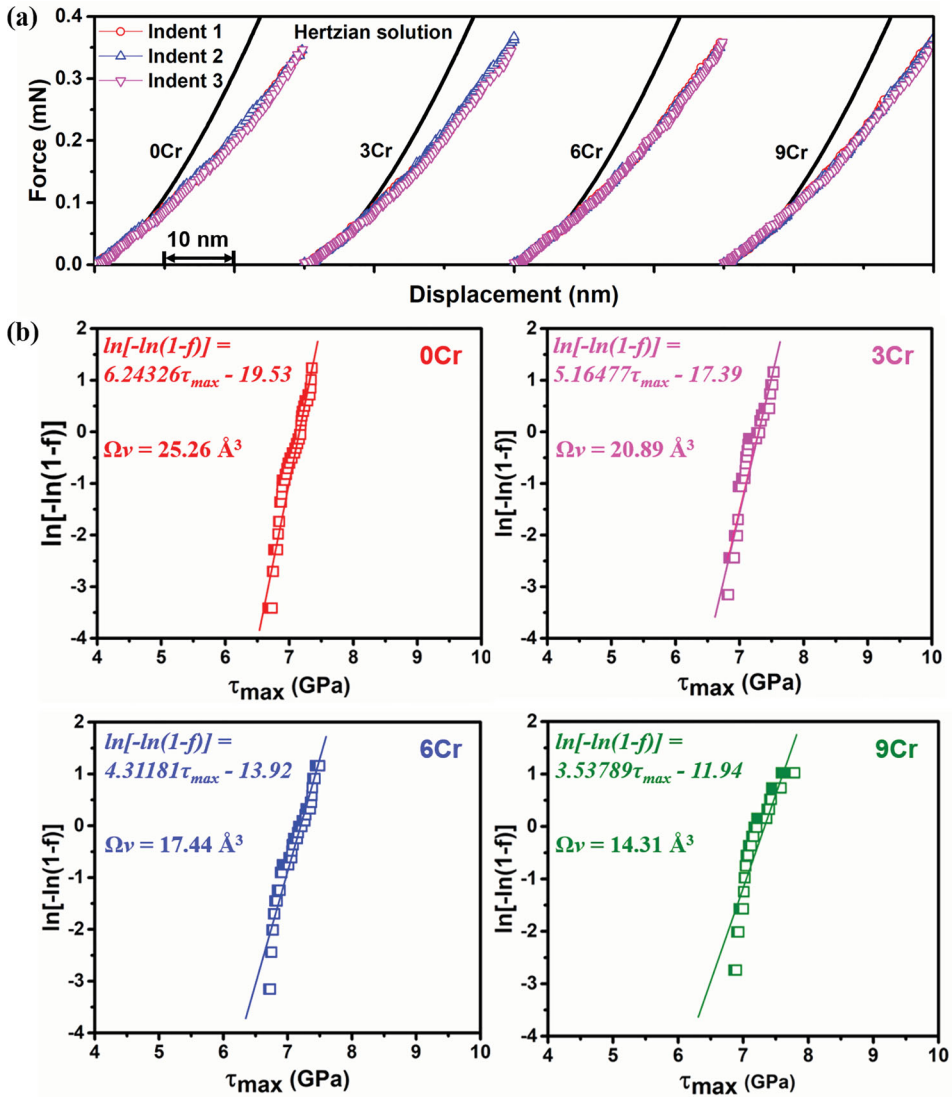

Figure 3. (a) Typical load-displacement (*P-h*) curves of austenite in the 0Cr, 3Cr, 6Cr and 9Cr samples; (b) corresponding relationship between *ln[-ln(1-f)]* and τ_{max} for deducing the activation volume through linear fitting.

An atomic volume Ω is $0.25a_0^3$ [10] where the lattice constant a_0 of $\sim$3.7 Å in austenite of the samples was measuerd by X-ray diffraction (XRD), as detailed in the Supplementary Information. Thus, the Ω of austenite is calculated as 12.66 Å^3, and the calculated Ω_v for dislocation nucleation in the 0Cr, 3Cr, 6Cr and 9Cr samples are 25.26 Å^3 (2.00 Ω), 20.89 Å^3 (1.65 Ω), 17.44 Å^3 (1.38 Ω) and 14.31 Å^3 (1.13 Ω), respectively.

As shown in Table 1, the measured τ_{max} is close to the theoretical shear strength ($\sim$1/10 μ, the shear modulus G of austenite is 70 GPa [5]). According to the relationship $M = \frac{\sigma_y}{\tau_0}$ [30], where M is the Taylor factor (3.06 [5]), σ_y is the yield strength (the σ_y of 0Cr sample is 836 MPa [17]) and τ_0 is the critical resolved shear stress for dislocation slip, τ_0 is calculated as $\sim$273 MPa. This value is much smaller than the measured τ_{max}. Thus, it can be considered that the incipient plasticity is controlled by dislocation nucleation [9–11,31], rather than the slip of pre-existing mobile dislocations. The obtained Ω_v values are in the range of 1–2 Ω, in between the Ω_v of $\sim$1 Ω for homogeneous nucleation and the several atomic volumes (2–5 Ω) required for heterogeneous nucleation via vacancy clusters or multiple-atom cooperative migration [8,10,11]. This suggests that the dislocation nucleation mechanism in all the investigated samples is heterogeneous nucleation via conventional atom-vacancy exchange [8,11].

Based on the results above, the intragranular premature κ-carbide has a negligible effect on the incipient plasticity, a phenomenon was also observed in Mo-added austenitic steels by J. Lee et al. [32]. Since the proposed heterogeneous dislocation nucleation is a stress-assisted thermally activated process [9,10,28], the effects of vacancy concentration and lattice inherent cohesion

Table 2. Quantitative compositions of austenite in the 0Cr, 3Cr, 6Cr and 9Cr samples (at. %) determined by EPMA.

Samples	Fe	Mn	Al	C	Cr
0Cr	60.45 ± 0.95	18.97 ± 0.33	15.00 ± 0.21	5.58 ± 0.33	–
3Cr	57.01 ± 0.91	19.04 ± 0.76	15.11 ± 0.06	5.83 ± 0.21	3.01 ± 0.14
6Cr	53.94 ± 0.83	19.34 ± 0.65	15.22 ± 0.15	6.12 ± 0.30	5.36 ± 0.40
9Cr	51.08 ± 0.49	19.92 ± 0.47	15.38 ± 0.12	6.30 ± 0.31	7.32 ± 0.15

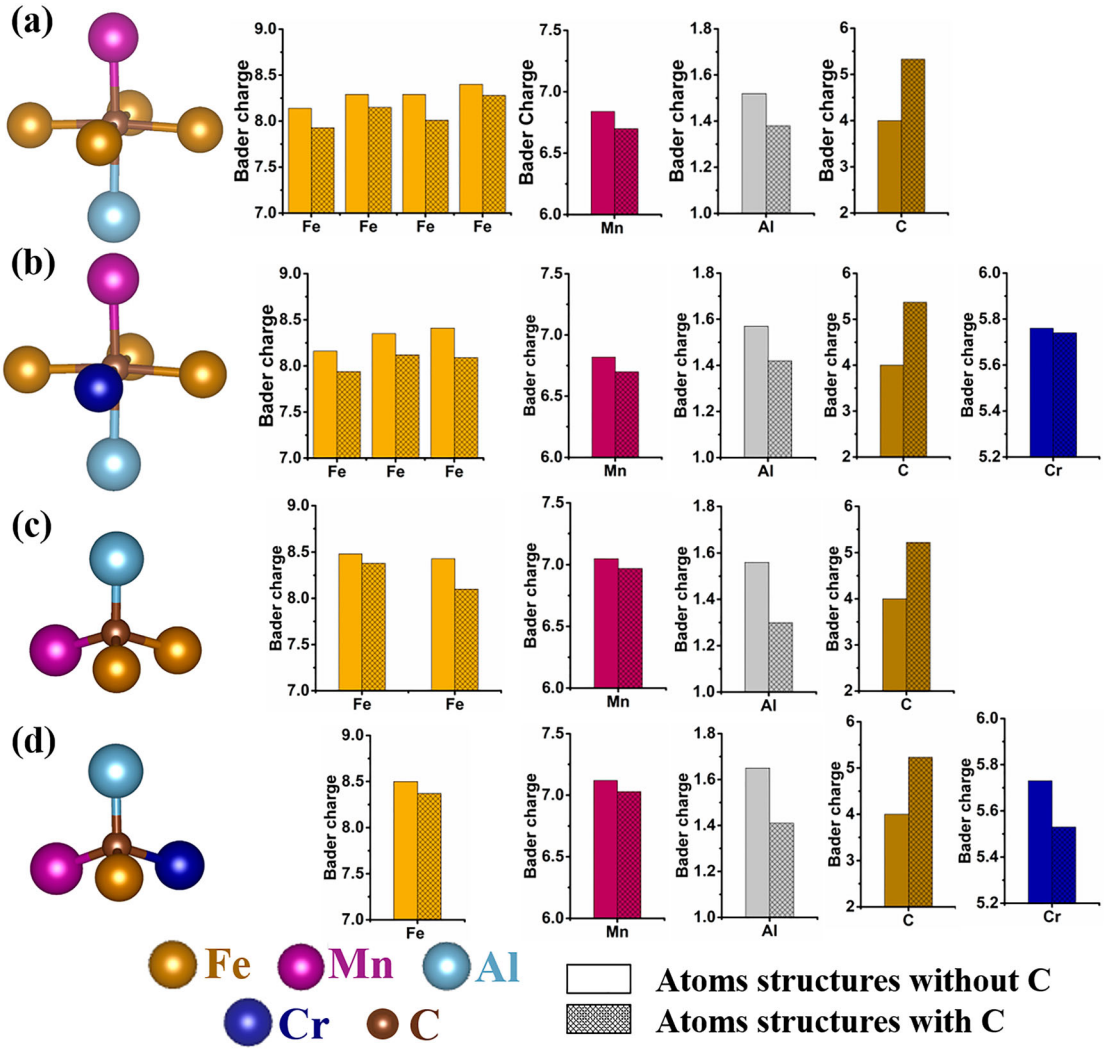

Figure 4. Proposed atomic structural models of the FCC structure used to calculate bader charge transfer between interstitial C atom and metallic atoms in the first neighboring coordination shell: (a) and (b) are the models with a C atom occupying a central octahedral site, while (b) has a Fe atom substituted by a Cr atom; (c) and (d) are the models with a C atom occupying a tetrahedral site, while (d) has a Fe atom substituted by a Cr atom.

must also be considered [9,10]. On the one hand, the same near-rapid solidification process resulted in nearly the same vacancy concentration in all four analyzed samples, which indicates a negligible effect of vacancy concentration variation. On the other hand, the solid-solution composition evaluation in austenite with Cr addition is an important factor affecting lattice inherent cohesion. Table 2 indicates that the Mn, Al and C elements contents in austenite all increase with Cr content. Metallurgically, the minor change of Mn and Al should have a limited impact on mechanical properties. However, the interstitial solutes generally have a huge impact on the incipient plasticity of different materials [9,10,33]. For example, interstitial solutes N/O have been found to induce local charge transfer enhancing lattice cohesion, which in turn increases the critical shear stress required for the onset of plasticity in NbTiZrHf HEA [9].

To further elucidate the lattice cohesion change caused by the increased C and Cr contents, the local charge transfer between interstitial C atom and surrounding

metallic atoms in FCC structure was calculated. The bader charge reflects the number of electrons localized near a particular atomic core [9], which is generally used as an effective tool to analyze the charge transfer among atoms. In this work, the interstitial C atoms are situated in octahedral and tetrahedral sites of the FCC structure as shown in Figure 4. Due to no detectable chemistry difference between the premature κ-carbide and austenite matrix (Figure 2), the structures where the C atoms are located in the octahedral site (Figure 4(a) and (b)) correspond to the premature κ-carbide. In addition, the Cr content change is considered by changing the number of nearest neighbor Cr atoms to C atom. It should be noted that the charge numbers on the outer layers of the ground states Fe, Mn, Al, Cr and C atoms are 8, 7, 3, 6 and 4, respectively. It is found that regardless of whether the interstitial C atom is in an octahedral or tetrahedral site, it always attracts significant electrons from its surroundings, decreasing thus the bader charges of the surrounding metallic atoms, as shown in Figure 4. However, the addition of Cr atoms has little effect on charge transfer. Note that the charge transfer between interstitial C atom and nearby metallic atoms is anticipated to transform the original metal–metal bond to ionic-like metal–carbon bonds, which results in enhanced atomic cohesion [9]. Thus, the calculated charge transfer suggests that the increased concentration of interstitial C atoms in austenite with Cr content (Table 2) significantly increases overall atomic cohesion, which in turn impedes dislocation nucleation events by increasing τ_{max} for incipient plasticity (Table 1).

4. Conclusion

In summary, we found that the incipient plasticity of all the studied samples (with and without intragranular premature κ-carbide) was dominated by a heterogeneous dislocation nucleation mechanism via atom-vacancy exchange. The decreased intragranular premature κ-carbide content and the concurrent slight increase of the maximum shear stress indicated the negligible effect of intragranular premature κ-carbide on incipient plasticity. However, the interstitial C content in austenite played a key role in dislocation nucleation. This was because the interstitial C atoms, as we show, induced local charge transfer leading to enhanced lattice cohesion, which in turn increased the shear stress for dislocation nucleation events.

Acknowledgements

The authors would like to express sincere thanks for the use of atom probe tomography (APT) in the Instrumental Analysis & Research Center at Shanghai University. The electron microscopy facilities in Lille, France, are supported by the Conseil Regional du Nord-Pas de Calais and the European Regional Development Fund (ERDF).

Disclosure statement

No potential conflict of interest was reported by the author(s).

Funding

This work was financially supported by the National Natural Science Foundation of China (No. 51974184), National MCF Energy R&D Program of China (No. 2018YFE0306102). Jianlei Zhang was grateful for his visiting Ph.D. project supported by the China Scholarship Council (Grant No. 201906890053).

References

[1] Chen SP, Rana R, Haldar A, et al. Current state of Fe-Mn-Al-C low density steels. Prog Mater Sci. 2017;89:345–391.
[2] Haase C, Zehnder C, Ingendahl T, et al. On the deformation behavior of κ-carbide-free and κ-carbide-containing high-Mn light-weight steel. Acta Mater. 2017;122:332–343.
[3] Yao MJ, Welsch E, Ponge D, et al. Strengthening and strain hardening mechanisms in a precipitation-hardened high-Mn lightweight steel. Acta Mater. 2017;140:258–273.
[4] Ardell AJ. Precipitation hardening. Metall Trans A. 1985;16(12):2131–2165.
[5] Welsch E, Ponge D, Hafez Haghighat SM, et al. Strain hardening by dynamic slip band refinement in a high-Mn lightweight steel. Acta Mater. 2016;116:188–199.
[6] Schuh CA, Mason JK, Lund AC. Quantitative insight into dislocation nucleation from high-temperature nanoindentation experiments. Nat Mater. 2005;4(8):617–621.
[7] Ye YX, Lu ZP, Nieh TG. Dislocation nucleation during nanoindentation in a body-centered cubic TiZrHfNb high-entropy alloy. Scr Mater. 2017;130:64–68.
[8] Wang SP, Xu J. Incipient plasticity and activation volume of dislocation nucleation for TiZrNbTaMo high-entropy alloys characterized by nanoindentation. J Mater Sci Technol. 2019;35(5):812–816.
[9] Ye YX, Ouyang B, Liu CZ, et al. Effect of interstitial oxygen and nitrogen on incipient plasticity of NbTiZrHf high-entropy alloys. Acta Mater. 2020;199:413–424.
[10] Gan KF, Yan DS, Zhu SY, et al. Interstitial effects on the incipient plasticity and dislocation behavior of a metastable high-entropy alloy: nanoindentation experiments and statistical modeling. Acta Mater. 2021;206:116633.
[11] Zhao YK, Park JM, Jang J-i, et al. Bimodality of incipient plastic strength in face-centered cubic high-entropy alloys. Acta Mater. 2021;202:124–134.
[12] Zambrano OA, Valdés J, Aguilar Y, et al. Hot deformation of a Fe-Mn-Al-C steel susceptible of κ-carbide precipitation. Mater Sci Eng A. 2017;689:269–285.
[13] Zhang RP, Zhao ST, Ding J, et al. Short-range order and its impact on the CrCoNi medium-entropy alloy. Nature. 2020;581:283–287.
[14] He BB, Liang ZY, Huang MX. Nanoindentation investigation on the initiation of yield point phenomenon in a medium Mn steel. Scr Mater. 2018;150:134–138.

[15] Zhang JL, Jiang YS, Zheng WS, et al. Revisiting the formation mechanism of intragranular κ-carbide in austenite of a Fe-Mn-Al-Cr-C low-density steel. Scr Mater. 2021;199:113836.
[16] Wang ZW, Lu WJ, Zhao H, et al. Formation mechanism of κ-carbides and deformation behavior in Si-alloyed FeMnAlC lightweight steels. Acta Mater. 2020;198:258–270.
[17] Zhang JL, Hu CH, Zhang YH, et al. Microstructures, mechanical properties and deformation of near-rapidly solidified low-density Fe-20Mn-9Al-1.2C-xCr steels. Mater Des. 2020;186:108307.
[18] Jeong S, Lee Y, Park G, et al. Phase transformation and the mechanical characteristics of heat-affected zones in austenitic Fe-Mn-Al-Cr-C lightweight steel during post-weld heat treatment. Mater Charact. 2021;177:111150.
[19] Kim KW, Park SJ, Moon J, et al. Characterization of microstructural evolution in austenitic Fe-Mn-Al-C lightweight steels with Cr content. Mater Charact. 2020;170:110717.
[20] Yang Y, Zhang JL, Hu CH, et al. Structures and properties of Fe-(8-16)Mn-9Al-0.8C low density steel made by a centrifugal casting in near-rapid solidification. Mater Sci Eng A. 2019;748:74–84.
[21] He W, Wang BL, Yang Y, et al. Microstructure and mechanical behavior of a low-density Fe-12Mn-9Al-1.2C steel prepared using centrifugal casting under near-rapid solidification. J Iron Steel Res Int. 2018;25:830–838.
[22] Seol JB, Haley D, Hoelzer DT, et al. Influences of interstitial and extrusion temperature on grain boundary segregation, Y-Ti-O nanofeatures, and mechanical properties of ferritic steels. Acta Mater. 2018;153:71–85.
[23] Li ZM, Körmann K, Grabowski B, et al. Ab initio assisted design of quinary dual-phase high-entropy alloys with transformation-induced plasticity. Acta Mater. 2017;136:262–270.
[24] Yao MJ, Pradeep KG, Tasan CC, et al. A novel, single phase, non-equiatomic FeMnNiCoCr high-entropy alloy with exceptional phase stability and tensile ductility. Scr Mater. 2014;72-73:5–8.
[25] Johnson KL. Contact mechanics. Cambridge, London: Cambridge university press; 1985.
[26] Mac Millan NH. The theoretical strength of solids. J Mater Sci. 1972;7(2):239–254.
[27] Oliver WC, Pharr GM. Measurement of hardness and elastic modulus by instrumented indentation: advances in understanding and refinements to methodology. J Mater Res. 2004;19(1):3–20.
[28] Schuh CA, Lund AC. Application of nucleation theory to the rate dependence of incipient plasticity during nanoindentation. J Mater Res. 2004;19(7):2152–2158.
[29] Lee J, Park S, Kim H, et al. Simulation of κ-carbide precipitation kinetics in aged low-density Fe-Mn-Al-C steels and its effects on strengthening. Met Mater Int. 2018;24:702–710.
[30] Sarkar A, Sanyal S, Bandyopadhyay TK, et al. Implications of microstructure, Taylor factor distribution and texture on tensile properties in a Ti-added Fe-Mn-Al-Si-C steel. Mater Sci Eng A. 2019;767:138402.
[31] Zhu C, Lu ZP, Nieh TG. Incipient plasticity and dislocation nucleation of FeCoCrNiMn high-entropy alloy. Acta Mater. 2013;61(8):2993–3001.
[32] Lee J, Kim H, Park SJ, et al. Correlation between macroscale tensile properties and small-scale intrinsic mechanical behavior of Mo-added Fe-Mn-Al-C lightweight steels. Mater Sci Eng A. 2019;768:138460.
[33] Sekido K, Ohmura T, Zhang L, et al. The effect of interstitial carbon on the initiation of plastic deformation of steels. Mater Sci Eng A. 2011;530:396–401.